

THERMAL RESISTANCE MEASUREMENTS OF A WELL-INSULATED WALL USING A CALIBRATED HOT BOX

R.R. Zarr D.M. Burch T.K. Faison C.E. Arnold

ABSTRACT

Thermal resistance measurements of a well-insulated residential wall are conducted using a calibrated hot box operated under a range of winter and summer climatic conditions. The wall consists of two insulated wood-frame sections with staggered framing, having a nominal thermal resistance of $R=27 \text{ h}\cdot\text{ft}^2\cdot\text{F}/\text{Btu}$ ($4.8 \text{ m}^2\cdot\text{K}/\text{W}$). The measured thermal resistance is examined as a function of mean wall temperature and compared with predictions using the ASHRAE parallel-path method, the ASHRAE isothermal-plane method, and a temperature-dependent thermal conductivity finite-difference model. Good agreement between measured and predicted values is obtained using both ASHRAE methods and the finite-difference model. At mean wall temperatures above 40 F (4.4°C), the ASHRAE parallel-path method tended to overpredict, while the ASHRAE isothermal-plane method tended to underpredict the overall thermal resistance. The effects of the compression of glass-fiber blanket insulation and nail penetrations on the overall thermal resistance are investigated.

INTRODUCTION

Upon completion of a series of calibration tests of the NBS Calibrated Hot Box (CHB) (Zarr et al. 1985), the National Bureau of Standards, through funding from the Department of Energy, initiated an effort to evaluate the thermal performance of a specially selected energy conserving wall. The CHB is a two-chamber facility (metering and climatic chamber) between which is mounted a wall specimen. Through accurate measurement of energy entering or leaving the metering chamber and using procedures established in ASTM C-976 "Standard Test Method for Thermal Performance of Building Assemblies by Means of a Calibrated Hot Box" (ASTM 1982), an energy balance is used to determine the thermal resistance of the test specimen. The NBS CHB is unique in that simultaneous measurements of heat, air, and mass transfer can be conducted, but for this investigation only the thermal resistance of the composite wall was measured.

The design of the wall system was selected by the National Bureau of Standards and the Department of Energy, with input from two industry groups, the National Association of Home Builders and the Manufactured Housing Institute. The intent was to select an energy conserving wall system that would have innovative construction features. The wall was made of two panels (back-to-back), each comprised of 2x3 framing studs 16 in (400 mm) on center, and provides an opportunity for automated assembly during manufacture. Moreover, the framing studs in the two panels are staggered when assembled, thereby reducing the thermal bridging through vertical framing members. An option also exists for installing additional thermal insulation between the two panels, converting this composite wall into a "superinsulated" wall.

R. R. Zarr, Mechanical Engineer, Center for Building Technology, NBS
D. M. Burch, Research Engineer, Center for Building Technology, NBS
T. K. Faison, Group Leader, Center for Building Technology, NBS
C. E. Arnold, Computer Programmer, Center for Building Technology, NBS

The tests conducted provide information for the design profession on the thermal performance of the wall system and provide comparisons between measured and predicted performance using several computational techniques. The methods of calculation accepted by the American Society of Heating, Refrigerating, and Air-Conditioning Engineers, Inc. (ASHRAE), the parallel-path and the isothermal-plane methods, are compared along with a more comprehensive finite-difference model. In the finite-difference model, the effect of highly conductive penetrations, such as nails penetrating the sheathing layer of the wall, is investigated. The thermal performance of the wall system is reported for a mean temperature varied over a range from 21 F (-6.1°C) to 101 F (38°C).

DESCRIPTION OF WALL SPECIMEN

The wall specimen consists of two separate wood-frame panels that form a staggered-stud wall system. The studs in opposite panels are offset, preventing a continuous thermal bridge through the vertical framing (see Figure 1). However, a continuous thermal bridge exists at the top and bottom sill plate.

The exterior panel framing consists of eleven 2x3 wood studs, 16 in (400 mm) on center. It was covered with a nominal 3/4 in thick (19 mm) sheet of foil-faced polyisocyanurate. To reduce air passage through the wall's insulation, an air infiltration retarder was placed over the polyisocyanurate sheathing. The air infiltration retarder is a 4 mil (0.10 mm) continuous sheet of high-density polyethylene fibers. The framing of the exterior panel was finished with a 1/2 in (13 mm) layer of plywood siding.

Glass-fiber blanket insulation was installed in the stud cavities of both panels. The nominal thermal resistance of the 3.5 in (89 mm) glass-fiber insulation was 11 h·ft²·F/Btu (1.94 m²·K/W). However, as the two panels were brought together, the glass-fiber insulation was compressed to fit in the stud cavity, 2.5 in (64 mm).

The framing of the interior panel consists of twelve 2x3 wood studs, 16 in (400 mm) on center, offset 8 in (200 mm) with respect to the framing of the exterior panel. The framing of the interior panel was covered with a 3 mil (0.08 mm) polyethylene vapor retarder and finished with a 1/2 in (13 mm) layer of gypsum board, that was taped, spackled, and painted.

The two panels as described above were fabricated by a local contractor and delivered to NBS, where they were assembled in the CHB 12-in-wide (300 mm) specimen support frame by NBS personnel. The interior panel was positioned one inch (25 mm) from the leading edge of the support frame and secured with rubber gasketing and aluminum angle. The exterior panel was then placed in the specimen support frame adjacent to the interior panel and also secured at its perimeter using rubber gasketing and aluminum angle.

The overall dimensions for the well-insulated wall were 8x15 ft (2.4x4.6 m), or 120 ft² (11.1 m²). The 8 foot height (2.4 m) was selected to more closely represent actual residential wall construction. Since the specimen support frame encompasses 150 ft² (13.9 m²), it was necessary to install a 2x15 ft (0.6x4.6 m) polystyrene "plug" between the top of the wall specimen and the support frame. The thickness of the plug was the same as the assembled wall, 6.9 in (175 mm). The joint between the plug and the specimen wall, as well as those between the wall and frame, was sealed with silicone-rubber caulk.

HEAT-TRANSFER PROPERTIES

Thermal Conductivities of Materials

The thermal conductivities for the individual components of the wall system, including the polystyrene insulation plug, the wood framing, the polyisocyanurate insulation, and the glass-fiber insulation, were measured in accordance with ASTM C-177 (ASTM 1985), using the NBS 1-meter Line Heat Source Guarded Hot Plate (GHP) over a range of mean temperatures. Further information on the NBS 1-meter Line Heat Source Guarded Hot Plate can be found in Rennex (1982). The results of these measurements are given in Figure 2. Each curve is a best-fit line through the measured data for the particular material. The thermal conductivity for gypsum board was taken to be a constant value of 0.0925 Btu/h·ft·F (0.160 W/m·K) (ASHRAE 1985).

The thermal conductivity of a wood-frame specimen was measured at several mean temperatures using the NBS Guarded Hot Plate. The specimen was not oven-dried prior to testing, and the measured conductivity values showed significant dependence on mean temperature. It was suspected that the moisture content of the wood changed as the specimen mean temperature was varied. For this reason, the uncertainty in the measured data was considered large, and the results are not included in Figure 2. Fortunately, the uncertainty in thermal conductivity for the wood framing has a very small effect on the overall thermal resistance calculations of the wall specimen.

Three additional GHP measurements were performed on a glass-fiber sample to determine its thermal conductivity as a function of density. The thermal conductivity of the glass-fiber blanket insulation shown in Figure 2 is based upon a compressed density of 0.70 lb/ft³ (11 kg/m³). Within each stud cavity, the glass-fiber insulation was compressed from 3.5 in (89 mm) to 2.5 in (64 mm). At a mean temperature of 75 F (24°C), the thermal resistance of the compressed blanket in each section is R-8.6 h·ft²·F/Btu (1.5 m²·K/W) compared to its uncompressed value of R-10.6 h·ft²·F/Btu (1.9 m²·K/W). Compressing the blanket insulation resulted in about a 19% reduction in its thermal resistance.

For the tests reported in the paper, the climatic chamber operated over a temperature range from -26 F (-32°C) to 130 F (54°C). At the low and high temperatures, the exterior materials in the wall were exposed to temperatures outside the range of the GHP measurements. At these temperatures, it was necessary to extrapolate to obtain thermal conductivity values.

Surface Heat-Transfer Coefficients

The inside and outside surface heat-transfer coefficients were 1.3 Btu/h·ft²·F (7.4 W/m²·K) and 2.5 Btu/h·ft²·F (14 W/m²·K), respectively. These values were determined by dividing the measured rate of heat transfer through the wall specimen by the product of the wall surface area and the measured temperature difference between the air and the surface.

DESCRIPTION OF THE CALIBRATED HOT BOX FACILITY

A schematic cross section of the NBS Calibrated Hot Box is given in Figure 3. The facility consists of three basic components: a metering chamber, a climatic chamber, and a specimen support frame. A brief description of the three components is given below.

For these tests, the well-insulated wall assembly was mounted in the support frame and inserted between the metering and climatic chambers. Thermal resistance measurements were made at four steady-state conditions. Typically, the metering chamber was operated at indoor conditions of 70 F (21°C), while the climatic chamber was maintained at one of four steady outdoor climate conditions. All tests were performed in accordance with the requirements of ASTM C-976 (ASTM 1985). The specimen heat transfer rate was determined from an energy balance of the metering chamber.

Metering Chamber

The metering chamber is a five-sided, highly insulated, rectangular enclosure. Its exterior walls are comprised of 15 in (380 mm) polyurethane board insulation providing a thermal resistance of R-91 h·ft²·F/Btu (R-16 m²·K/W). Surrounding the exterior surface of the metering chamber is a uniform temperature water jacket guard, maintained at the same temperature as the air in the metering chamber. Due to the very large wall resistance and the absence of a temperature gradient, the rate of heat transfer through the exterior walls is quite small (i.e., measurements are typically less than 0.5 W [Zarr et al. 1985]).

Within the metering chamber, air is conditioned by a 2,400 W electric-resistance heater and a 0.65 ton (2,300 W) cooling coil. The cooling coil, when required, is operated at a constant flow rate and maintained above the dewpoint temperature of the metering chamber air. Air is circulated by a 1/4 hp (187 W) propeller blower. The air may be delivered to either the top or bottom of the specimen through air diffusers, which are designed to deliver a uniform distribution of air across the specimen wall. The air speed can be varied by changing the speed of the blower.

Climatic Chamber

The climatic chamber is a second five-sided highly insulated, rectangular enclosure, the same size as the metering chamber. Its walls have no water jacket guard, but there is a full 18-in-thickness (460 mm) of polyurethane board insulation providing a thermal resistance of $108 \text{ h}\cdot\text{ft}^2\cdot\text{F}/\text{Btu}$ ($19 \text{ m}^2\cdot\text{K}/\text{W}$).

Air for the climatic chamber is conditioned by an external system having a 7,500 W electric-resistance heater and a 5.8 ton (21,000 W) refrigeration system (R502). A portion of this air is diverted to a two-stage rotating-drum desiccant dryer that removes water vapor from the air. The purpose of the dryer is to maintain a sufficiently low dewpoint temperature so that frost will not accumulate and diminish the refrigeration coil capacity. Air is circulated to the climatic chamber by a 7.5 hp (5,600 W) vaneaxial blower. As in the case of the metering chamber, conditioned air may be delivered at either the top or bottom of the specimen through air diffusers. The air speed can be adjusted by changing the speed of the blower or changing the the spacing between the specimen and baffle.

Specimen Support Frame

The 12-in-wide (300 mm) specimen support frame is capable of mounting wall specimens having a thickness up to 10 in (250 mm), and an overall area of $10\times 15 \text{ ft}^2$ ($3.0\times 4.6 \text{ m}^2$). The frame consists of 18-in-thick (460 mm) polyurethane board insulation covered with 0.067 in (1.7 mm) fiber-glass reinforced plastic (FRP) skin to provide structural support. The design was engineered to minimize the heat transfer through the specimen frame while still maintaining adequate structural support for the specimen. The calibrated hot box also has a 24-in-wide (610 mm) specimen support frame not utilized in the present study.

INSTRUMENTATION AND MEASUREMENT TECHNIQUE

The primary purpose of the calibrated hot box is to measure the overall energy transfer (Q_{sp}) through a wall specimen. Essentially, Q_{sp} is equal to the net energy gain to the metering chamber (Q_{in}) minus the energy transfer (Q_{fl}) through the specimen support frame, known as the flanking loss. The net energy gain of the metering chamber is determined by performing a steady-state energy balance on the metering chamber. The flanking loss was empirically measured as part of the calibration procedure, and can be predicted using a finite-difference computer model that is discussed in detail in the CHB calibration report (Zarr et al. 1985).

For the energy balance of the metering chamber, the energy gains into the metering chamber (Q_{in}) are equated to the energy losses (see Figure 4), or;

$$Q_{in} = Q_h + Q_{bl} = Q_{sp} + Q_{fl} + Q_{cc} + Q_i + Q_{box} \quad (1)$$

where

- Q_h = energy input by electric heater;
- Q_{bl} = energy input by blower;
- Q_{cc} = energy removed by cooling coil;
- Q_i = energy transfer due to air infiltration;
- Q_{box} = energy loss through exterior walls of the metering chamber;
- Q_{sp} = energy loss through specimen, and
- Q_{fl} = flanking loss.

The terms Q_h , Q_{bl} , Q_{cc} , Q_i , and Q_{box} are measured directly. Their method of measurement and associated uncertainty has been described previously (Zarr et al. 1985). The flanking loss (Q_{fl}) is determined using a finite-difference computer model.

The surface-to-surface thermal resistance of the specimen (R) is determined from the relation:

$$R = A \cdot (T_{sm} - T_{sc}) / Q_{sp} \quad (2)$$

where

A = surface area of the specimen;

T_{sm} = specimen surface temperature on the metering chamber side, and

T_{sc} = specimen surface temperature on the climatic chamber side.

The specimen surface temperature is measured using a 40-junction thermopile referenced to a platinum resistance thermometer embedded in an isothermal bronze block. The thermopile temperature's uncertainty is ± 0.05 F (± 0.03 K). From the previous calibration study, the overall uncertainty for the measurement of the specimen thermal resistance was estimated to be $\pm 2.0\%$.

The center of the wall specimen was instrumented with five heat-flux transducers (HFT), evenly spaced over a 16 in (400 mm) section at the mid-height of the wall. The HFTs were placed on the interior side of the wall and adhered to the surface with a silicone-rubber compound. Each HFT was masked with a rubber material similar in composition to the HFT.

R-VALUE CALCULATIONS

The total heat transfer through the wall specimen was analyzed by dividing the wall specimen into five regions, as shown in Figure 5. Considerations of symmetry reduced the number of regions analyzed to three: a center, a side, and a bottom/top region. In each region, a characteristic cross section(s) of the region was identified and the heat transfer per length of section calculated. The characteristic cross sections that were used in the analysis are given in Figure 6.

The total heat transfer (Q_{sp}) through the wall specimen was computed from the relation:

$$Q_{sp} = L_c \cdot Q_c + 2 \cdot (L_s \cdot Q_s) + 2 \cdot (L_{bt1} \cdot Q_{bt1} + L_{bt2} \cdot Q_{bt2} + L_{bt3} \cdot Q_{bt3}) \quad (3)$$

where

L = length of the heat-transfer region, and

Q = heat transfer per length of region.

Here the subscripts c, s, and bt refer to the center, side, and bottom/top regions, respectively. Note that there are three types of bottom/top regions (see Figure 6).

The thermal resistance of the wall specimen, surface to surface, (R) was computed by the relation:

$$R = A \cdot (T_i - T_o) / Q_{sp} - 1/h_i - 1/h_o \quad (4)$$

where

A = surface area of the specimen;

T_i = inside air temperature;

T_0 = outside air temperature;

h_i = inside surface heat-transfer coefficient, and

h_o = outside surface heat-transfer coefficient.

The heat-transfer rates through the characteristic regions were computed using the finite-difference and ASHRAE methods described in the next sections.

Finite-Difference Model

The heat-transfer rates through each of the characteristic sections were computed using a finite-difference computer program described in Zarr et al. 1985. This computer program is capable of predicting two-dimensional heat transfer through any arbitrarily shaped body that can be represented by rectangular homogeneous areas. Arbitrary boundary conditions, including adiabatic surfaces, convective surfaces, constant temperature surfaces, or conductive surfaces may be specified.

Each of the characteristic sections for the wall (illustrated in Figure 6) were divided into homogeneous areas. The thermal conductivity for each area was determined from its thermal conductivity relation given above, based upon the mean temperature of the area. The finite-difference program divides each of the areas into a nodal grid structure, using a specified number of nodes, and then develops heat-balance equations for each node. The resulting system of heat-balance equations is solved by the Gauss-Seidel iteration method.

For an initial condition, all nodal temperatures are a constant specified value. The temperatures of the nodes are then solved iteratively, and this process is repeated until a specified level of convergence for the heat transfer through the section is achieved. The heat transfer through a section was computed by summing the convective heat transfer for the nodes located along the inside surface. The finite-difference node structure and resulting isotherm (i.e., lines of constant temperature) pattern for the center region are illustrated in Figure 7.

The effect of nail penetrations on the overall thermal resistance of the wall specimen was analyzed using a finite-difference model described in the appendix. This finite-difference program computes a heat-transfer coefficient for a metal cylindrical penetration through a building component. When this heat-transfer coefficient is multiplied by the temperature difference across the building component, the excess heat transfer caused by the penetration is obtained.

The wall specimen contained three types of nail penetrations: gypsum board nails, sheathing nails, and siding nails. Here the type of nail denotes the material attached by the nail. The sheathing and siding nails were initially conjectured to have a significant effect on the overall thermal resistance because in both cases a large number of very conductive metal rods penetrated the polyisocyanurate sheathing, a layer having large thermal resistance. There were 127 sheathing nails and 174 siding nails. These two cases were analyzed using the finite-difference model for metal cylindrical penetrations. Since the gypsum board nails penetrated a highly conductive layer, they were not analyzed.

Figures 8a and 8b show cross sections for the cylindrical penetration models used for the sheathing and siding nails. Isotherms predicted by the finite-difference model are superimposed on each cross section. At a mean temperature of 35 F (1.7°C), the heat-transfer coefficient (H) was found to be 1.5×10^{-4} Btu/h·F (8.0×10^{-5} W/K) for a sheathing nail and 2.2×10^{-4} Btu/h·F (1.2×10^{-4} W/K) for a siding nail.

The overall specimen heat-transfer coefficient (H_{sp}) with nail penetrations may be predicted by the relation:

$$H_{sp} = U'_{sp} \cdot A_{sp} + N_{sh} \cdot H_{sh} + N_{si} \cdot H_{si} \quad (5)$$

where

U'_{sp} = thermal transmittance of wall specimen without nail penetrations;

A_{sp} = surface area of specimen;
 N_{sh} = number of sheathing nails;
 H_{sh} = heat-transfer coefficient for sheathing nails;
 N_{si} = number of siding nails, and
 H_{si} = heat-transfer coefficient for siding nails.

The thermal resistance (R) of the wall system with nail penetrations is defined by the relation:

$$R = A_{sp}/H_{sp}. \quad (6)$$

At a mean temperature of 35 F (1.7°C), the thermal resistance of the wall specimen was determined to be 22.8 h·ft²·F/Btu (3.98 m²·K/W) without nail penetrations. Using Equations 5 and 6, the thermal resistance of the wall specimen with nail penetrations was calculated to be 22.6 h·ft²·F/Btu (3.94 m²·K/W). Therefore, the presence of the nail penetrations produced a reduction in thermal resistance of 0.2 h·ft²·F/Btu (0.04 m²·K/W), or 0.9%.

ASHRAE Methods

The two accepted ASHRAE methods that utilize one-dimensional heat transfer theory to model the wall specimen sections as a thermal resistance network are the parallel-path method and the isothermal-plane method. Both methods are illustrated in Figure 9 for the center region.

In the case of the parallel-path method, parallel heat-flow paths are assumed and the thermal resistance of each material layer is summed. An area-weighted average of the path conductances is used to determine the overall thermal resistance.

For the isothermal-plane method, isothermal planes are assumed at the interface of each material layer, allowing each layer to have one or more parallel heat-flow paths for the materials. The overall thermal resistance is determined by analysis of the resistance network.

Using each method to calculate an overall thermal resistance, the heat-transfer rates through the characteristic cross sections given in Figure 6 were predicted. An area weighted form of Equation 3 was used to compute the total specimen heat transfer (Q_{sp}).

RESULTS

Specimen Thermal Resistance

In Figure 10, the measured thermal resistance of the wall specimen is plotted as a function of mean wall temperature and compared with predictions using the ASHRAE isothermal-plane method, the ASHRAE parallel-path method, and a temperature-dependent thermal conductivity finite-difference model. The CHB measurements are average values obtained for a steady 12-hour period. An uncertainty band of ±2.0% based upon the calibration (Zarr et al. 1985) is included with each data point without the metering chamber cooling coil in operation. For the summer test at a mean temperature of 101 F (38°C), errors in the coil energy transfer measurement propagate such that a 2% uncertainty in the coil measurement becomes a ±6% uncertainty in the R-value determination.

The finite-difference solution, with and without nail penetrations, is shown as solid lines. At a mean temperature of 35 F (1.7°C), the presence of the nail penetrations lowered the predicted finite-difference value by 0.2 h·ft²·F/Btu (0.04 m²·K/W), as described in the in the previous section. The ASHRAE methods are shown as individual data points.

At mean temperatures below 50 F (10°C), both the CHB measurements and finite-difference solution show the specimen thermal resistance (R-value) deviates from a linear dependence of mean temperature. This is explained by examining the nonlinear thermal conductivity behavior of polyisocyanurate at temperatures below 40 F (4.4°C) (see Figure 2). At mean temperatures below 40 F (4.4°C), it is observed that the thermal conductivity of polyisocyanurate increases as the mean temperature is reduced. It was hypothesized that the encapsulated refrigerant in the polyisocyanurate condenses, increasing its thermal conductivity at low temperatures. Since the polyisocyanurate sheathing represents 19% of the overall specimen R-value, its increasing thermal conductivity at low temperatures would explain the departure from linearity of the specimen thermal resistance.

The ASHRAE methods show the thermal resistance of the specimen as a linear function of the mean specimen temperature. These methods use thermal conductivity values based on mean specimen temperature. For mean specimen temperatures above 40 F (4.4°C), the ASHRAE methods adequately predict the specimen thermal resistance. At mean temperatures above 40 F (4.4°C), the isothermal-plane method tends to underpredict the specimen thermal resistance, while the parallel-path method tends to overpredict the specimen thermal resistance.

Two additional ASHRAE calculations were performed using the design values listed in the 1985 ASHRAE Fundamentals. For the isothermal-plane method, an R-value of 20.3 h·ft²·F/Btu (3.58 m²·K/W) was calculated, and for the parallel-path method, an R-value of 21.4 h·ft²·F/Btu (3.77 m²·K/W) was calculated. Design data at a mean temperature of 75 F (23.9°C) were used for these calculations.

Specimen Heat Flux for Center Section of Specimen

Figure 11a shows the cross section where the five specimen heat-flux transducers were located. The measured heat flux for each HFT is plotted in Figure 11b along with the heat flux predicted by the finite-difference solution at the interior surface for the center region. The maximum difference (12%) between the two values occurs at HFT #1. The profile shows that despite the staggered stud spacing some thermal bridging is present due to the vertical framing members.

SUMMARY AND CONCLUSIONS

The CHB measured values for the wall's thermal resistance were plotted as a function of mean wall temperature and compared to several predictive models. The measured thermal resistance of the wall specimen varied from R-22.8 h·ft²·F/Btu (4.02 m²·K/W) to R-18.5 h·ft²·F/Btu (3.26 m²·K/W) for a mean wall temperature ranging from 21 F (-6.1 °C) to 101 F (38 °C). The thermal resistance of the well-insulated wall specimen was approximately twice that of conventional wood-frame construction.

Wall thermal resistances were predicted using a temperature-dependent thermal conductivity finite-difference solution, the ASHRAE isothermal-plane method, and the ASHRAE parallel-path method. In the finite-difference solution and the ASHRAE methods, thermal conductivity relations as a function of temperature based upon guarded-hot-plate measurements were used in the analysis. Thermal resistances predicted by the finite-difference solution and both ASHRAE methods were in good agreement with the CHB measurements. These results indicate that wall thermal resistance of wood-frame construction can be accurately predicted using existing models.

The compression of glass-fiber blanket insulation from 3.5 in (89 mm) to 2.5 in (64 mm) was found to reduce its thermal resistance by about 19%. At a mean temperature of 35 F (1.7°C), the presence of nail penetrations in the wall specimen's sheathing reduced its overall thermal resistance by 0.2 h·ft²·F/Btu (0.04 m²·K/W), or about 0.9%.

REFERENCES

- ASHRAE. 1985. ASHRAE Handbook-1985 Fundamentals. Atlanta: American Society of Heating, Refrigerating, and Air-Conditioning Engineers, Inc, pp. 23.1-23.22.
- ASTM. 1985. 1985 Annual Book of ASTM Standards. "Standard test method for thermal performance of building assemblies by means of a calibrated hot box." Vol 04.06, ASTM C976-82. Philadelphia: American Society for Testing and Materials, pp. 660-683.
- ASTM. 1985. 1985 Annual Book of ASTM Standards. "Standard test method for steady-state thermal transmission properties by means of the guarded hot plate." Vol 04.06, ANSI/ASTM C177-76. Philadelphia: American Society for Testing and Materials, pp. 21-54.
- Rennex, B.G. 1982. "Error analysis for the NBS 1016 mm guarded hot plate." Journal of Thermal Insulation, Vol. 7, pp. 18-51.
- Zarr, R.R.; Burch, D.M.; Faison, T.K.; Arnold, C.E.; and O'Connell, M.E.; 1985. "Calibration of the NBS calibrated hot box." (ASTM STP XXX in press).

ACKNOWLEDGMENTS

The authors thank the Department of Energy for financial sponsorship of this effort. Also, the authors thank Brian Rennex and Thomas Somers for their work in providing thermal conductivity values for materials used in the wall specimen. Finally, the authors thank Mike O'Connell and Paul Shoback for their technical assistance in preparation of the specimen.

APPENDIX

A Heat-Transfer Analysis Of Nail Penetrations Through The Wall Specimen

INTRODUCTION

This appendix presents a finite-difference analysis of the heat transfer through sheathing and siding nail penetrations of the wall specimen. The sheathing and siding nails were believed to have a significant effect on the overall thermal resistance because a large number of these nails penetrated the polyisocyanurate sheathing, a layer having a large thermal resistance.

PHYSICAL GEOMETRY AND HEAT-TRANSFER PARAMETERS USED IN THE ANALYSIS

The physical geometries for cases with sheathing and siding nails are given in Figures 8a and 8b in the text. The thicknesses and thermal conductivities for the material components are given in Table A-1. The outside diameter of the cylindrical section was taken to be 2 in (51 mm). A sheathing nail consisted of 1.5 in long (38 mm), 0.12 in diameter (3.0 mm) shaft with a 0.37 in diameter (9.4 mm), and a 0.040 in thick (1.01 mm) head. A siding nail consisted of a 2.5 in long (64 mm), 0.11 in diameter (2.8 mm) shaft with a 0.20 in diameter (5.1 mm), and 0.041 in thick (1.04 mm) head. The nails were comprised of steel having a thermal conductivity of $26 \text{ h}\cdot\text{ft}^2\cdot\text{F}/\text{Btu}$ ($45 \text{ m}\cdot\text{K}/\text{W}$).

The surface heat-transfer coefficients were taken to be $2.5 \text{ Btu}/\text{h}\cdot\text{ft}^2\cdot\text{F}$ ($14 \text{ W}/\text{m}^2\cdot\text{K}$) at the exterior surface and $1.4 \text{ Btu}/\text{h}\cdot\text{ft}^2\cdot\text{F}$ ($7.9 \text{ W}/\text{m}^2\cdot\text{K}$) at the interior surface. These surface heat transfer coefficients corresponded to the actual conditions during the calibrated-hot-box tests. For the analysis, the outdoor and indoor air temperatures were taken to be 0.0 F (-18°C) and 70 F (21°C), respectively.

FINITE DIFFERENCE THEORY

The physical geometries shown in Figures 8a and 8b were subdivided into 800 nodal subregions. The node structure for the physical geometries is similar in principle to the previous example. A computer program was developed that generates a heat balance equation containing the following elements:

$$Q_{\text{COND},R} + Q_{\text{COND},L} + Q_{\text{COND},U} + Q_{\text{COND},D} + Q_{\text{SURF}} = 0 \quad (\text{A-1})$$

where

$Q_{\text{COND},R}$ = conduction from the adjoining node to the right;

$Q_{\text{COND},L}$ = conduction from the adjoining node to the left;

$Q_{\text{COND},U}$ = conduction from the adjoining node above;

$Q_{\text{COND},D}$ = conduction from the adjoining node below, and

Q_{SURF} = surface heat transfer.

At interior nodes, convection is not present ($Q_{\text{CONV}} = 0$), and the following heat balance equation is generated:

$$A_R \cdot (T - T_R) / \Delta r + A_L \cdot (T - T_L) / \Delta r + A_U \cdot (T - T_U) / \Delta y + A_D \cdot (T - T_D) / \Delta y = 0 \quad (\text{A-2})$$

where

T = temperature at node;

r = radial coordinate;

y = height coordinate;

A_R = surface area at the right side of the node;

A_L = surface area at the left side of the node, and

A_U, A_D = surface area at top and bottom of the node, respectively.

The surface areas A_R and A_L are the sides of a cylinder, and the surface areas A_U and A_D represent the top and bottom of a cylinder. The subscripts R, L, U, and D refer to the right, left, upper, and lower nodes, respectively. At the boundaries of a region, where a region adjoins another solid region, an equation similar to Equation A-2 is generated, but this equation is different in that it shares conduction elements with other regions. When a surface boundary condition is specified, the heat transfer (Q_{SURF}) to the surface is predicted from Newton's law of cooling, or:

$$Q_{\text{SURF}} = h \cdot A_T \cdot (T_s - T_a) \quad (\text{A-3})$$

where

h = surface heat-transfer coefficient;

A_T = surface area of top of a cylindrical region;

T_s = surface temperature, and

T_a = air temperature.

The head of the nail was modeled as a metal skin. That is, it was treated as having thermal resistance in the lateral direction but none in the longitudinal direction. This assumption is equivalent to neglecting the very small temperature gradient across the head of the nail. This is accomplished mathematically by including a thermal conductance for the head of the nail in parallel with that of the adjoining region.

The shaft of the nail was modeled as having only longitudinal thermal resistance (i.e., the thermal resistance in the lateral direction was neglected). In the finite-difference equations for nodes adjoining the shaft of the nail, a thermal conductance for the shaft was incorporated into the equations. The heat transfer through the wall section was determined by summing Q_{SURF} for the nodes along a convective boundary.

The resulting linear system of algebraic equations was solved by the method known as Gauss Seidel iteration. In this method, the temperatures of the nodes are solved iteratively. This process is repeated until a specified level of convergence for the heat transfer through the wall section is achieved. To get such a process started, all temperatures are initially assumed to be a specified constant value.

As a check on the validity of the numerical solution, a heat balance on each material comprising the wall section was computed. The residual heat transfer for each of the materials was found to be less than 10^{-4} Btu/hr (3×10^{-5} W).

RESULTS

Isotherms are superimposed on the cross sections given in Figures 8a and 8b. By making use of the fact that heat flows perpendicularly to the isotherms, we see that the head and shaft of the nail gather heat laterally from adjoining materials and conduct this heat through the insulation layer of polyisocyanurate.

A heat-transfer coefficient for the nail penetration was defined by the following relation:

$$H = (Q - Q') / (T_o - T_i) \quad (A-4)$$

where

Q = total heat transfer through wall section with nail penetration;

Q' = total heat transfer through wall section without nail penetration;

T_o = outdoor temperature, and

T_i = indoor temperature.

Note that, when the heat-transfer coefficient (H) is multiplied by the temperature difference ($T_i - T_o$), the excess heat transfer caused by the nail penetration is obtained. Heat-transfer coefficients (H) for the cases of sheathing and siding nails are given in the text.

TABLE A-1

Heat-Transfer Parameters

Material Component	Thickness		Thermal Conductivity	
	in	mm	Btu/h·ft·F	W/m·K
Wood Siding	0.578	14.7	0.0607	0.105
Polyisocyanurate	0.714	18.1	0.0136	0.0235
Wood Framing	2.47	62.8	0.0585	0.101
Glass-Fiber Ins.	2.47	62.8	0.0229	0.0396
Gypsum Board	0.496	12.6	0.0925	0.160

WELL-INSULATED WALL SPECIMEN

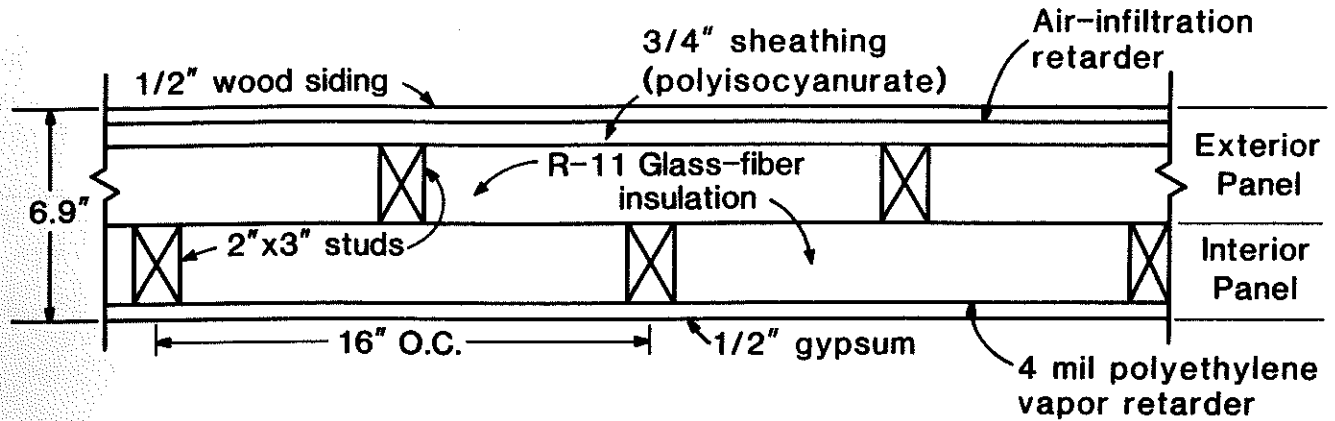


Figure 1. Cross-sectional view of wall specimen

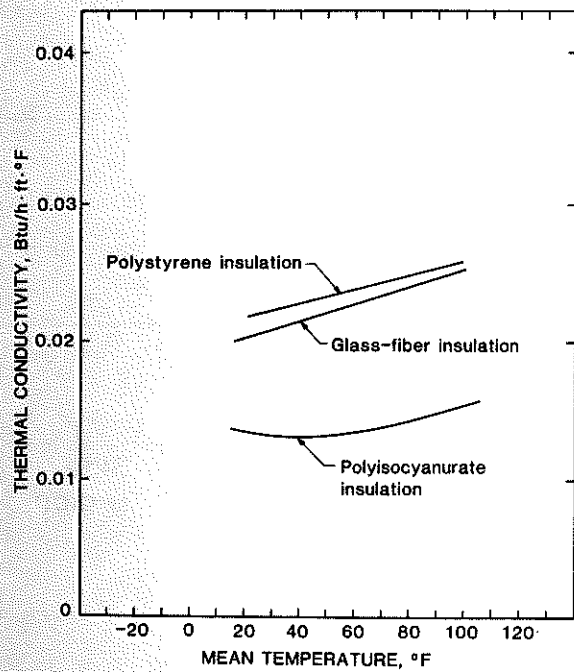


Figure 2. Thermal conductivity of wall specimen components plotted as a function of mean temperature

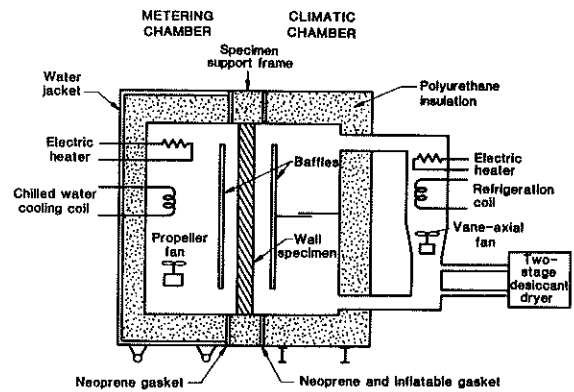
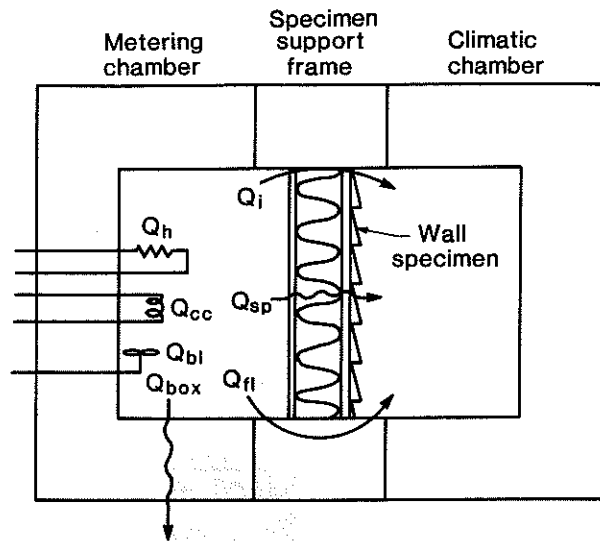


Figure 3. Schematic cross section of the calibrated hot box



$$Q_{in} = Q_h + Q_{bl} = Q_{sp} + Q_{fl} + Q_{cc} + Q_i + Q_{box}$$

- where
- Q_h = electric energy consumed by heater
 - Q_{bl} = electric energy consumed by blower
 - Q_{cc} = heat removed by the cooling coil
 - Q_{sp} = heat transfer through the specimen
 - Q_{fl} = flanking loss
 - Q_{box} = heat transfer through the box walls
 - Q_i = heat transfer due to infiltration

Figure 4. Steady-state energy balance for the metering chamber

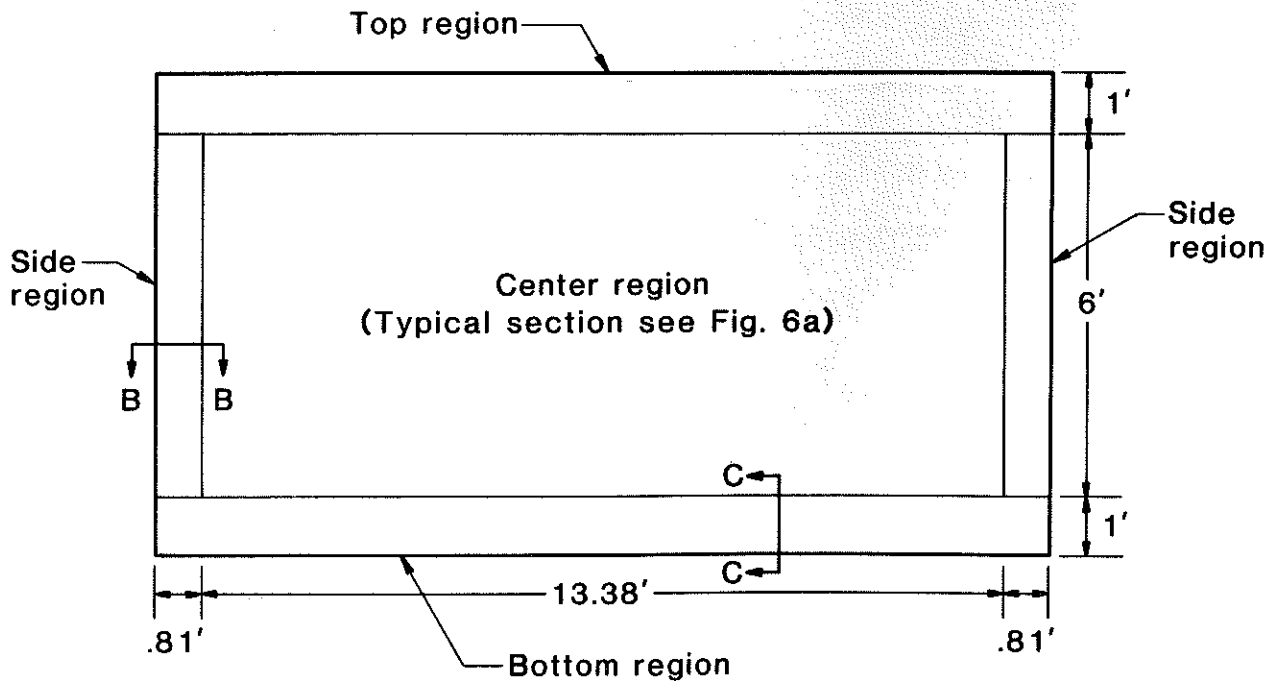


Figure 5. Heat transfer regions for wall specimen (front view)

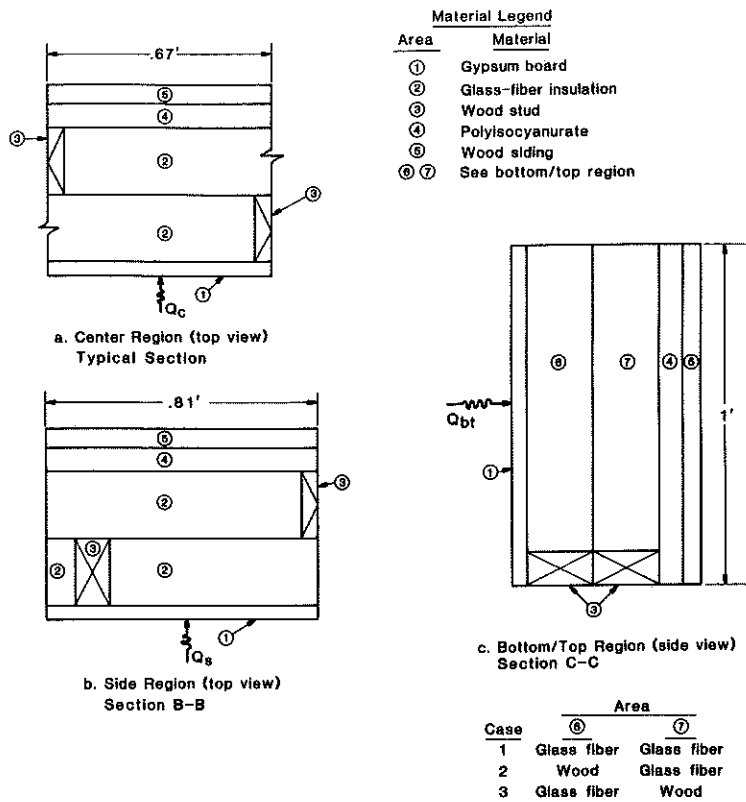


Figure 6. Characteristic cross sections of wall specimen

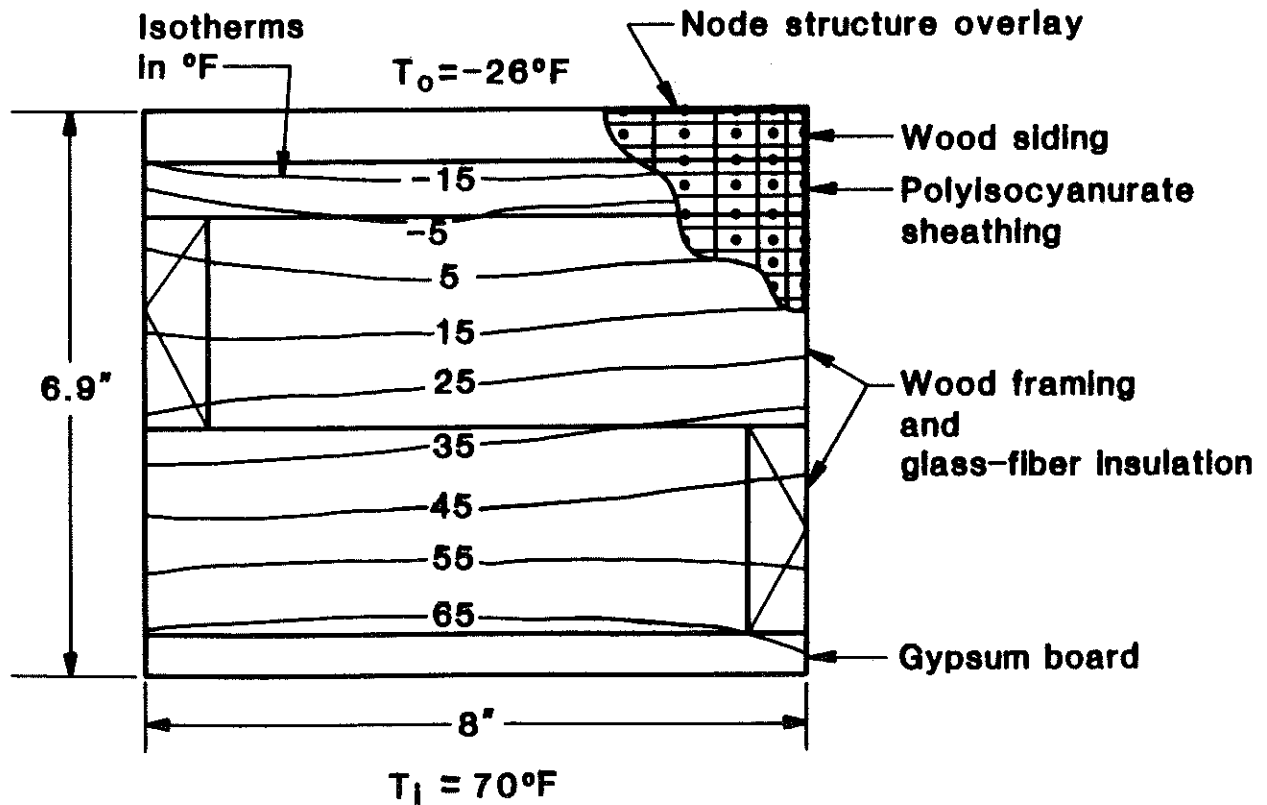


Figure 7. Finite-difference node mesh and isotherms for center region

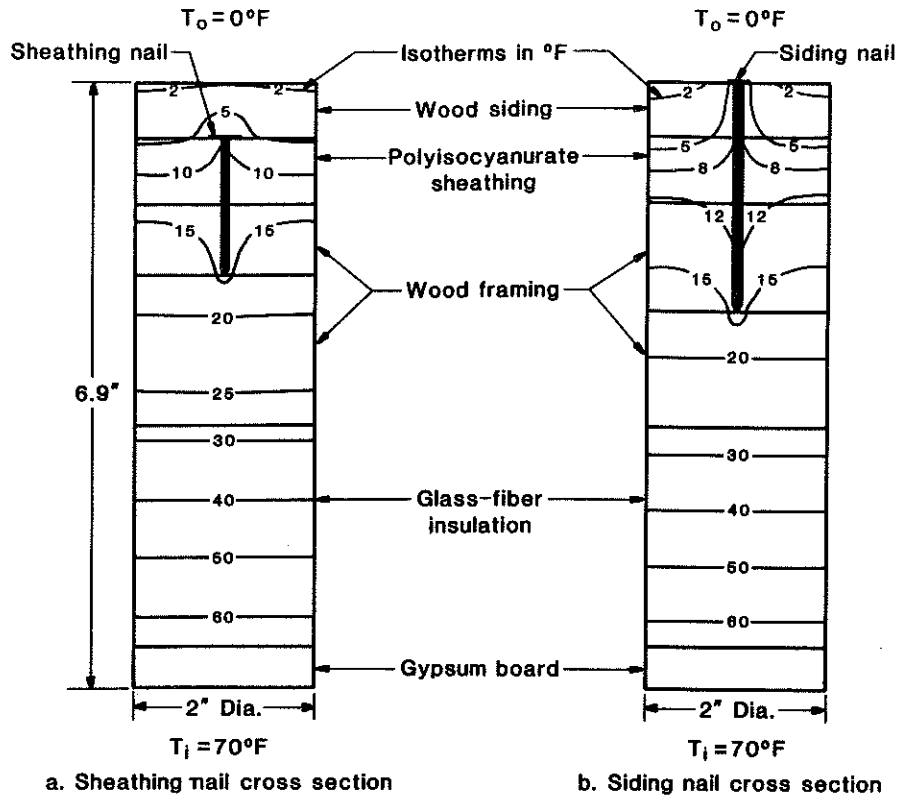
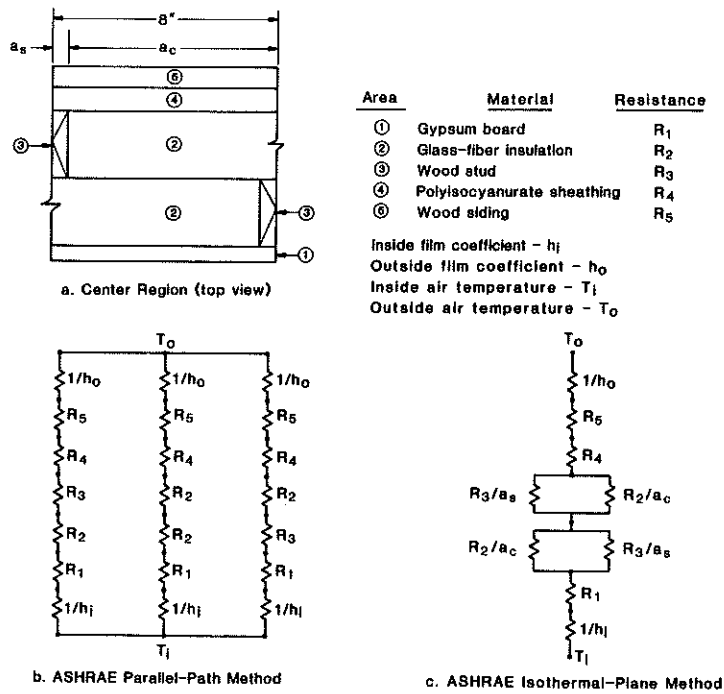


Figure 8. Isotherms for cylindrical metal-penetration models



$$Q_c = \frac{A(T_i - T_o)}{R_T}$$

where, Q_c = heat transfer through center region
 A = area of center region
 R_T = overall thermal resistance of center region

Figure 9. One-dimensional heat-transfer models for center region

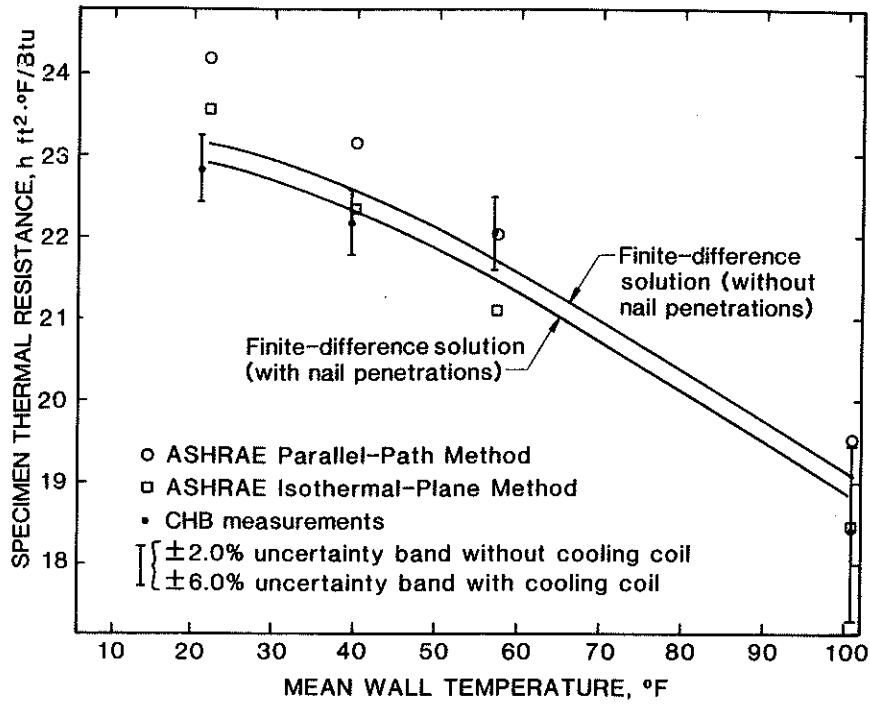
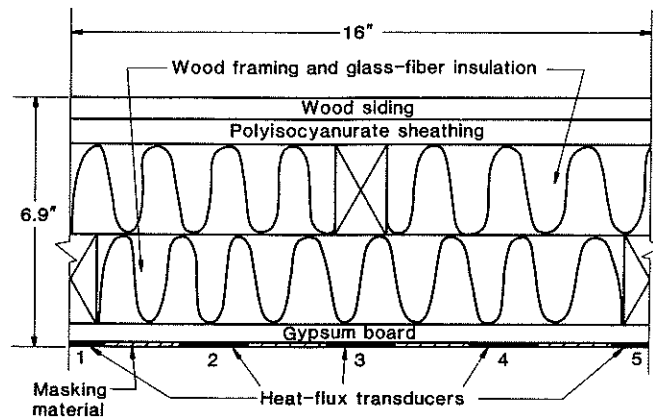


Figure 10. Specimen thermal resistance plotted as a function of mean wall temperature



Location of specimen heat-flux transducers

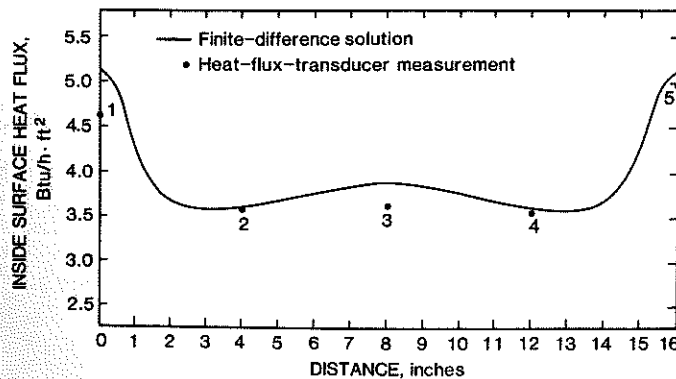


Figure 11. Variation of the interior heat flux for the center region. Temperature difference across specimens, 96 F (50°C)